P8A.13 BRIGHTBAND IDENTIFICATION FROM VERTICAL PROFILE OF REFLECTIVITY

Jian Zhang[1], Carrie Langston[1], and Kenneth Howard[2]

[1]Cooperative Institute for Mesoscale Meteorological Studies, The University of Oklahoma, and
[1,2] NOAA/OAR National Severe Storms Laboratory, Norman, OK

1 INTRODUCTION

The term “bright band” used in radar meteorology refers to a layer of abnormally high reflectivity observations associated with the melting of aggregated snow. The phenomenon has been recognized since the very early ages of radar meteorology (e.g., Ryde 1946; Austin and Bemis 1950; Wexler and Atlas 1956; Lhermitte and Atlas 1963). The abnormally high reflectivity causes significant overestimation in radar precipitation estimates if appropriate correction is not applied (E.g., Koistinen 1991; Joss and Lee 1995; Andrieu and Creutin 1995; Kitchen et al. 1994; Smyth and Illingworth 1998; Westrick et al. 1999; Vignal et al. 1999, 2000; Seo et al. 2000; Vignal and Krajewski 2001; Germann and Joss 2002; Bellon et al. 2005; and references therein). Thus it is important to identify those areas of radar observations that are affected by the bright band layer. Knowledge of the bright band layer can also provide information about microphysical processes in the precipitation (e.g., Takeda and Fujiyoshi 1978; Stewart et al. 1984; Willis and Heymsfield 1989) and can lead to more accurate rainfall estimation by using appropriate Z-R relationships (e.g., Smith 1986; Huggel et al. 1996). In addition, the height of the bright band layer is an indication of 0°C isotherm and can be useful in identifying areas of potential icing hazards for aviation and in the data assimilation for numerical weather prediction models.

Various techniques have been developed for automated identification of bright band layer from radar observations. Fabry and Zawadzki (1995) studied bright band structure using a vertically pointing radar with very high temporal (2 s) and spatial (15 m) resolution. They analyzed reflectivity profiles from five different precipitation regimes in the area of Montreal, Canada and found that the melting of ice particles is not the only mechanism for bright band. The shape, density and fall speed of the ice particles also play important roles for the existence of a bright band. Sanchez-Diezma et al. (2000) examined impacts of radar volume scan sampling strategies on the observed bright band peak intensity and depth using simulated data, and based on the simulation results, they developed a bright band identification (BBID) algorithm. Gourley and Calvert (2003) developed an automated BBID scheme for the base level reflectivity data from WSR-88Ds (Weather Surveillance Radar - 1988 Doppler) and compared the bright band top and bottom heights obtained from the BBID scheme with model 0°C temperature height and with observations from a vertically pointing radar. The BBID scheme by Gourley and Calvert (2003) applies to each bin column of the base level reflectivity data, and then averages the bin-by-bin bright band information (e.g., bottom and top heights) over space and time. The current paper presents an alternative BBID scheme for the WSR-88D, which is based on the mean vertical profiles of reflectivity (VPRs). By using the VPRs instead of the base data, the scheme is largely simplified and more computationally efficient. The new BBID scheme is similar to what was proposed in Sanchez-Diezma et al. (2000), but is adapted to the WSR-88D scan strategies and is evaluated using the radars in the conterminous United States (CONUS).

*Corresponding Author address: Jian Zhang, 120 David L Boren Blvd, Norman, OK 73072, e-mail: jian.zhang@noaa.gov.

2 ALGORITHM DESCRIPTIONS

The BBID algorithm presented here comprises of the following three steps:

1) Convective and stratiform precipitation segregation;
2) Computation of volume scan mean VPRs for different precipitation groups; and
3) Bright band identification from stratiform VPRs.

Detailed description of each step is provided below.

2.1 Convective and stratiform precipitation segregation

The occurrence of the bright band is most often associated with stratiform precipitation (e.g., Stewart et al. 1984; Willis and Heymsfield 1989; Fabry and Zawadzki 1995). To obtain accurate measure of the bright band layer, a volume scan of reflectivity data are segregated into convective and stratiform precipitation type for every bin column in spherical coordinates. A radar bin column is identified as convective if one of the following conditions is met: a) a reflectivity at any height in the column is greater than 50 dBZ or b) a reflectivity is greater than 30 dBZ at –10°C height or above. Temperature soundings are obtained from hourly analyses of an operational numerical weather prediction model. All the radar bin columns that are not identified as convective are classified as stratiform. Figure 1 shows an example precipitation type and the associated composite reflectivity field for a squall line event that occurred on May 24, 2007 across Oklahoma and Kansas. The red and purple areas are identified as being convective precipitation in the leading edge of the squall line and light blue and yellow areas are associated with the trailing stratiform precipitation region (Fig.1b). The consistency between the two fields indicates that the simple convective/stratiform segregation scheme is effective.

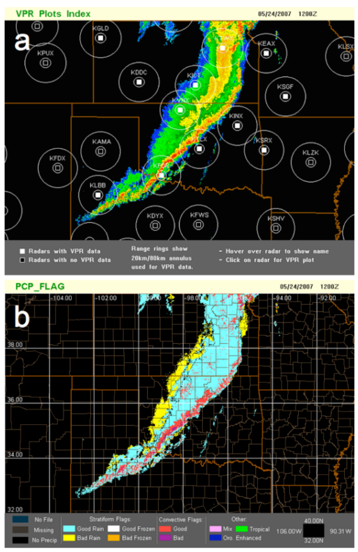

Fig. 1 a) Composite reflectivity and b) precipitation type fields valid at 12:00UTC on 24 May 2007. The white circles in panel *a* represent the bounds of the annular region where VPRs are computed.

2.2 Volume scan mean VPRs

Two mean VPRs are computed for each radar volume scan, one for convective and another for stratiform precipitation. A volume scan of reflectivity data are quality controlled to remove non-precipitation echoes. The quality control scheme uses a neural network approach that is based on horizontal and vertical reflectivity structure (Lakshmanan et al., 2007). There are pre- and post-processing steps in addition to the neural network component in the quality control scheme. The pre- and post-processing utilize spatial and temporal reflectivity filters and heuristic rules based on radar scan mode and environmental data to remove specific non-precipitation echoes such as speckles, sun strobes, biological returns, and anomalous propagations due to nocturnal radiation cooling near the surface. After the quality control, reflectivity observations from all tilts in an annular region between two pre-defined ranges (r_1 and r_2, see Fig.2) are divided into two groups based on precipitation types (see section 2.1). The annular region is chosen to be sufficiently close to the radar so that high vertical resolution of reflectivity can be obtained in the final VPRs. In addition, the region needs to be away from the radar to avoid the cone of silence and ground clutter in the immediate vicinity of the radar. Empirical values of 20 and 80 km are used for r_1 and r_2 (Fig.2), respectively, based on studies with ~2 years of WSR-88D data.

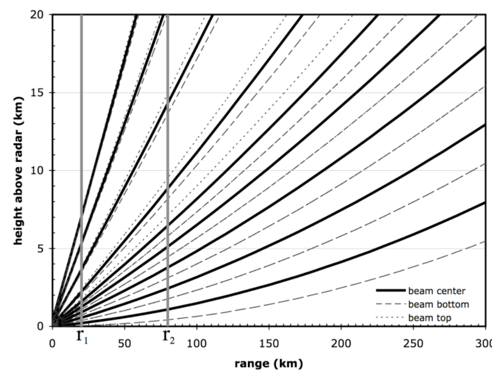

Fig. 2 WSR-88D beam propagation path (VCP21) under standard atmospheric refractive conditions. The bold black vertical lines indicate the ranges between which volume scan reflectivity data are used to derive vertical profiles of reflectivity.

Reflectivity data for each precipitation type are further grouped into evenly spaced vertical layers according to the central height of the reflectivity bins. The number of vertical layers, N, is determined by two pre-specified height parameters, h_0 and h_t (default = 0.5 and 20km above radar level, respectively), which represent the bottom and top of the domain where VPR is derived. The height of each vertical layer, h[k], is defined as the following:

$$N = (h_t - h_0)/\Delta h + 1 \qquad (1)$$

$$h[k] = h_0 + k^*\Delta h; \quad k = 0, N-1. \qquad (2)$$

Here k is the layer index, and Δh (default = 200m) is the thickness of each layer. Within each layer the mean and standard deviation of all the reflectivity observations are computed as following:

$$\overline{Z}[k] = \frac{1}{M}\sum_{i=1}^{M} Z[i]; \quad k = 0, N-1. \qquad (3)$$

$$\sigma_{Z[k]} = \frac{1}{M}\sqrt{\sum_{i=1}^{M}\left(Z[i] - \overline{Z}\right)^2}; \quad k = 0, N-1. \qquad (4)$$

Here $\overline{Z}$[k] is the mean reflectivity in the k^{th} layer and $\sigma_{Z[k]}$ is the standard deviation. M is the total number of reflectivity observations in the k^{th} layer, i is the index of reflectivity observations, and Z[i] is an observed reflectivity value within the k^{th} layer. A reflectivity bin is considered to be in the k^{th} layer if:

$$h[k] - 0.5*\Delta h \le h_Z[i] \le h[k] + 0.5*\Delta h; \qquad (5)$$

where $h_Z[i]$ is the height at the center of the i^{th} reflectivity bin.

Two rules are applied to assure a representative and robust VPR: i) only reflectivities higher than a threshold (Z_0) are included in VPR, and ii) a minimum number (M_0) of reflectivity observations with $Z[i] \ge Z_0$ are required within each height layer to get a valid mean reflectivity for the VPR. Both Z_0 and M_0 are adaptable parameters (default = 10 dBZ and 10, respectively). If at any given layer a valid $\overline{Z}[k]$ cannot be obtained, then a linear interpolation using valid $\overline{Z}$ values from layers above and below is applied to get an alternative $\overline{Z}[k]$. The interpolation is limited within a depth of $\Delta h_{intp} = \pm$ 1km (adaptable). A 3-point running mean is applied to the final VPR to reduce random fluctuations.

Figure 3 shows example VPRs from the same squall line event as shown in Fig.1. The stratiform VPRs (Figs.3a and 3b) are different than the convective VPRs (Figs.3c and 3d) because of the different microphysical processes in the two precipitation regimes. The bright band feature is apparent in the stratiform VPRs and the peak of the bright band corresponds very well to the 0°C height level derived from the Rapid Update Cycle (RUC) model analysis (Figs.3a and 3b). There is no bright band feature in the convective VPRs (Figs.3c and 3d). The automated BBID algorithm is developed based on the mean stratiform VPRs and the next section presents the detail of the algorithm.

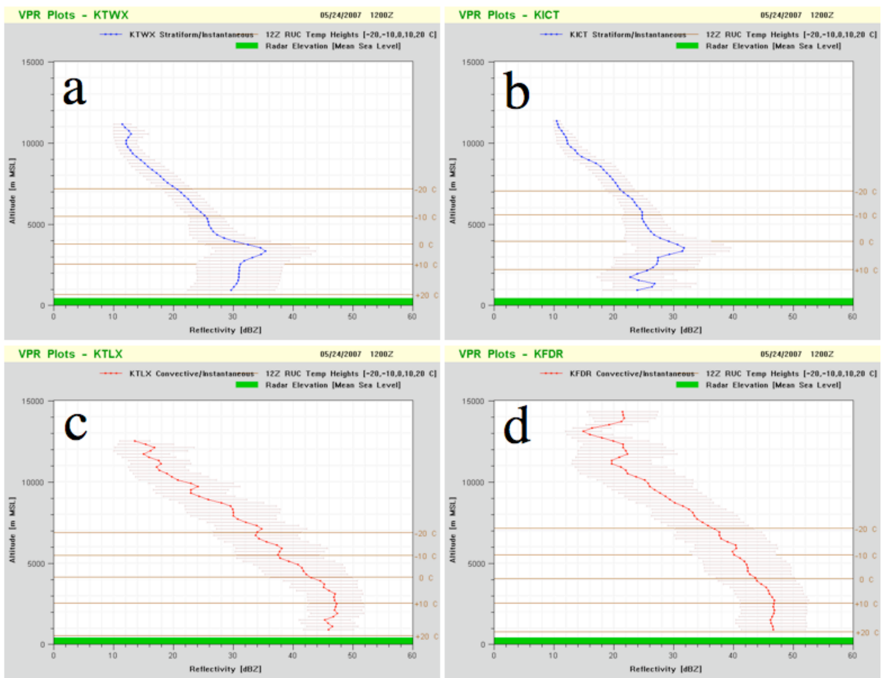

Fig. 3 Example volume scan mean VPRs valid at 12:00UTC on 24 May 2007: a) and b) stratiform VPRs from KTWX and KICT radars, respectively; c) and d) convective VPRs from KTLX and KFDR radars, respectively. The bold horizontal brown lines represent the heights of 20, 10, 0, -10, -20°C temperatures at the radar sites. The thin brown bars represent standard deviations of reflectivity values that went into the mean VPRs.

2.3 Bright band identification

Bright band identification is based on the volume mean stratiform VPRs and a temperature sounding at the radar site. The automated BBID is based on a conceptual model shown in many previous studies such as Fabry and Zawadzki (1995) and Sanchez-Diezma et al. (2000) and includes three steps:

1) Find the local maximum near the freezing level in the VPR;
2) Check for existence of a bright band; and
3) If a bright band exists, find the bottom and top heights of the bright band layer.

The search for the local maximum in the VPR starts from 500 m above the model 0°C height at the radar site and continues downward. The 500 m cushion is used to account for uncertainties in the model 0°C height due to infrequent and sparse upper air sounding observations. Once the local maximum is identified, the algorithm finds the height above (below) the maximum level where reflectivity monotonically decreases by a given percentage (default = 10%) of the maximum reflectivity. A bright band existence is determined if the following criteria are met:

$$h_a - h_b \le D_0; \quad (6)$$
$$h_a - h_m \le D_1; \quad (7)$$
$$h_m - h_b \le D_1; \quad (8)$$

Here h_m is the height of the maximum reflectivity; h_a (h_b) is the height above (below) the maximum reflectivity level where the reflectivity decreases by 10% of the maximum. D_0 and D_1 are adaptable parameters that are constrained by the depth and symmetry of the bright band layer. The parameter D_1 is equivalent to the parameter ΔH in Fabry and Zawadzki (1995). Based on their simulation results and our studies of several thousands of VPRs from the WSR-88Ds, an empirical value of 1.0 km is used for D_1 and 1.5 km is used for D_0. Note that these values are dependent on radar scan strategies and the vertical resolution of reflectivity observations. The D_0 and D_1 parameters will require tuning if the algorithm is applied to different radar than the WSR-88Ds.

If a bright band exists, its top and bottom heights are then set to h_a and h_b, but with the following constraints:

$$h_a - h_m \le D_t; \quad (9)$$
$$h_m - h_b \le D_b; \quad (10)$$

The default values for D_t and D_b are 500 m and 700 m, respectively. The difference values are used to account for the different slopes of VPRs above and below the bright band peak level (Fig.4). The increasing rate of reflectivity above the bright band peak is usually larger than the decreasing rate of reflectivity below (Fabry and Zawadzki 1995). The sum of D_t and D_b defines an upper limit to the total depth of the bright band layer. Previous studies with very high-resolution vertically pointing radar data showed that the bright band layer is usually less than a few hundreds meters thick (Fabry and Zawadzki 1995). However, simulation results from Sanchez-Diezma et al. (2000) using a 10-cm radar with 1° beam width showed that the impact of the bright band layer on radar observations can be as thick as 2 km. Figure 4 illustrates this bright band expanding effect due to the radar beam spreading with range. When the radar is operating in VCP-21, a bright band layer of 500 m thick can impact radar bins over a depth of 1 to 1.5 km within the range of 80 km (see Fig.4). Beyond the range of 100 km, the expanding of the bright band is even larger (Fig.4). Meanwhile the peak intensity will decrease with range because of the smoothing effect of the radar power density function (Sanchez-Diezma 2000).

Since the current BBID scheme uses reflectivities near the radar to identify the bright band layer, the resultant depth of the bright band will be smaller than the depth influenced by the bright band at the far range (Fig.4). Therefore, the bright band depth information should be used with caution when applied at far ranges. Note that the values of D_t and D_b are also adaptive parameters depending on the radar data resolution and need to be re-tuned for different radar network.

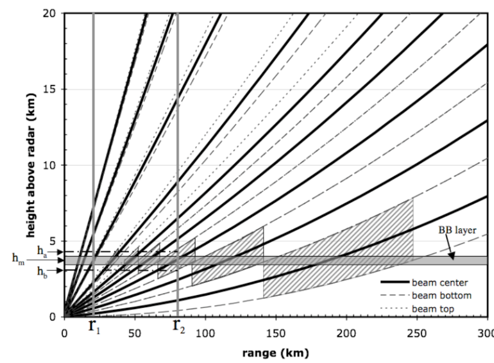

Fig. 4 An illustration of bright band layer observations in the context of the WSR-88D volume scan patter (VCP) 21. The solid grey area indicates the bright band layer as if it is observed by very high-resolution vertically pointing radar. The hatched area indicates the areas where WSR-88D observations in VCP 21 may be affected by the bright band. The height of h_m represents the peak reflectivity height of the bright band layer, and h_a and h_b represent the bright band top and bottom heights that are determined by the current BBID scheme (see text).

3 CASE STUDY

The BBID scheme has been implemented and tested on ~130 radars in the CONUS in real-time system using the National Mosaic and QPE system (NMQ, http://www.nmq.nssl.noaa.gov). Figures 5 and 6 provide examples of BBID results from a wide spread wintertime stratiform precipitation event occurred on 24 January 2007 in the south Texas area. The precipitation lasted for extended period of time and was observed by several radars (Fig.5). The bright band layer was detected from several radars in the region and over a long period of time (Fig.6). The height of the bright band top identified by the BBID algorithm correlates very well with the 0°C height from the RUC (Rapid Update Cycle) model analysis at each radar site, indicating that the BBID scheme is robust.

The bright band top heights from radar data are available every 5 minutes while the model analysis is only available every hour (Fig.6), and the upper air sounding is even less frequent (every 12 hours). The bright band top height identified from the KHGX site showed similar trend to the bright band top from the KEWX site and both time series had physically realistic smooth transitions over time. However, the model's 0°C height near the KHGX site showed some large temporal variations at times around 3Z and 11Z, and after 16Z. These variations appeared to be less physically realistic than those in the bright band top time series. Therefore the bright band top height identified from radar data can be potentially used to improve the model temperature and cloud analyses.

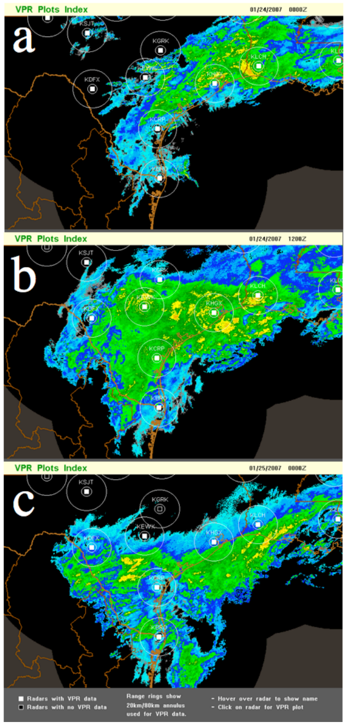

Fig. 5 Composite reflectivity for a winter precipitation event occurred in the south Texas region (*a*) at 00Z on 1/24/2007; (*b*) at 12Z on 1/24/2007; and (*c*) at 00Z on 1/25/2007.

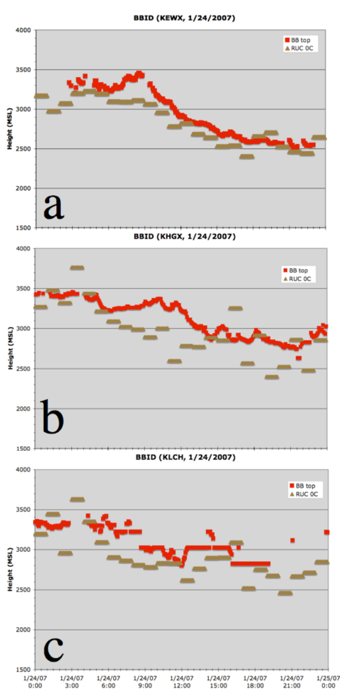

Fig. 6 Time series of the bright band top height (red squares) identified from the BBID algorithm and RUC analysis 0°C height (brown line segments) from (a) KEWX, (b) KHGX), and (c) KLCH radars in Texas on 24 January 2007.

Figure 7 shows time series of bright band top, bottom and the peak level heights from the same event as in Fig.6. The average difference between bright band top and bottom heights is around 1 km, indicating that the constraint for bright band depth (i.e., D_t+D_b =1.2 km) is reasonable. The bright band top and bottom heights delineate areas where radar reflectivities are inflated. Radar quantitative precipitation estimation (QPE) is usually based on the reflectivity observations in the lowest tilt. If the lowest radar tilt intersects this layer, then an adjustment (reduction) is necessary to mitigate potential overestimation when the data are used for precipitation estimation.

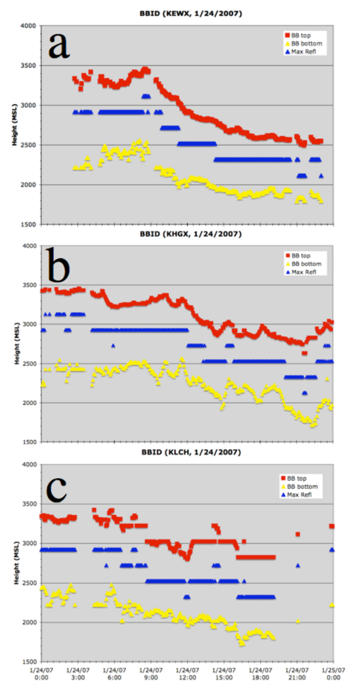

Fig. 7 Time series of the bright band top (red squares), bottom (yellow triangles), and peak reflectivity (blue triangles) heights identified from the BBID algorithm from (a) KEWX, (b) KHGX), and (c) KLCH radars in Texas on 24 January 2007.

Figure 8 shows a squall line that passed across Oklahoma and Kansas on 24 May 2007 (Fig. 8a) and the associated ratio bias map of the hourly radar precipitation estimation against rain gauge observations (Fig. 8b). Overestimations of 50 – 100% occurred within the trailing stratiform region as outlined by the red polygon in Figs.8a and 8b. The BBID results from four different radars (Fig.9) showed that a bright band layer was detected in the stratiform region. The bright band bottom height ranges around 3.1 km (Fig.9b) above mean sea level in the northern part of the squall line to

3.5 km (Figs.9c and 9d) in the southern part. The region outlined by the polygon is on the average about 125 km away from the surrounding radars. At this distance, the top of the lowest tilt is ~ 3 km above radar level (Fig.2), or, ~ 3.4km above mean sea level (the area average terrain height is about 400 m above mean sea level). Therefore the lowest tilts from the surrounding radars were affected by the bright band layer and the subsequent radar precipitation estimates were inflated due to the high reflectivity values associated with the bright band. This case demonstrates the importance of the bright band information to improve radar QPEs accuracy.

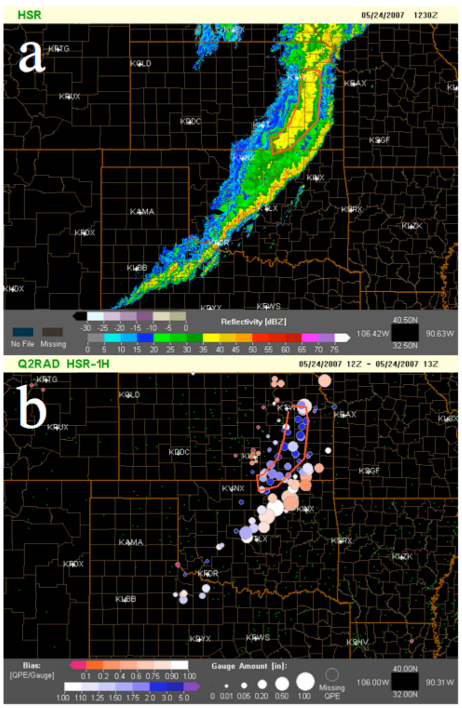

Fig. 8 Hybrid scan reflectivity at 12:30UTC (a) and bias of the hourly radar precipitation estimates against co-located hourly rain gauge observations ending at 13:00UTC on 24 May 2007.

4 SUMMARY

A new automated bright band identification technique has been developed. The new technique is based on vertical profiles of reflectivity (VPRs) from WSR-88D radar data and a background atmospheric temperature profile. The new BBID scheme is evaluated using over 2 years of WSR-88D data from ~130 radars in the CONUS. It was found that VPR-based BBID scheme is very effective in identifying the bright band layer from WSR_88D data and can provide valuable information for accurate radar QPEs and for numerical weather prediction model data assimilation.

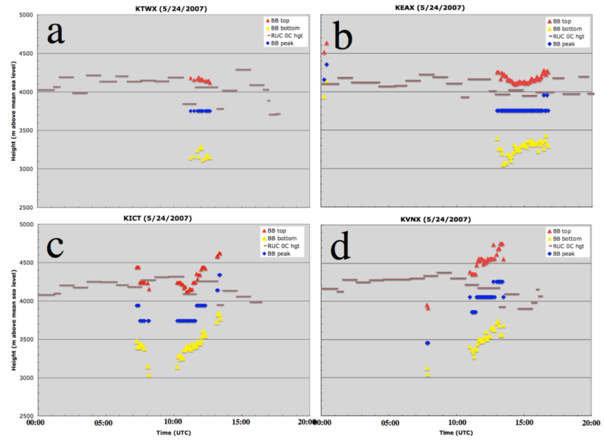

Fig. 9 Bright band top (red triangles), bottom (yellow triangles), beak (blue diamonds), and RUC 0C height (brown line segments) from KTWX, KEAX, KICT, and KVNX radars on 24 May 2007.

Acknowledgements

Major funding for this research was provided under the Federal Aviation Administration (FAA) Aviation Weather Research Program Advanced Weather Radar Technologies Product Development Team MOU and partial funding was provided under NOAA-University of Oklahoma Cooperative Agreement #NA17RJ1227, U.S. Department of Commerce.

This research is in response to requirements and funding by the Federal Aviation Administration (FAA). The views expressed are those of the authors and do not necessarily represent the official policy or position of the FAA.

References

Andrieu, H., and J. D. Creutin, 1995: Identification of vertical profiles of radar reflectivity for hydrological applications using an inverse method. Part I: Formulation. *J. Appl. Meteor.*, **34,** 225 – 239.

Austin, P. M., and A. C. Bemis, 1950: A quantitative study of the "bright band" in radar precipitation echoes. *J. Meteor.,* **7,** 145 – 151.

Bellon, A., G.-W. Lee, and I. Zawadzki, 2005: Error statistics of VPR corrections in stratiform precipitation. *J. Appl. Meteor.*, **44**, 998-1015.

Fabry, F., and I. Zawadzki, 1995: Long-term radar observations of the melting layer of precipitation and their interpretation. *J. Atmos. Sci.,* **52,** 838 – 851.

Germann, U., and J. Joss, 2002: Mesobeta profiles to extrapolate radar precipitation measurements above the Alps to the ground level. *J. Appl. Meteor*., **41**, 542-557.

Gourley, J. J., and C. M. Calvert, 2003: Automated detection of the bright band using WSR-88D radar data. *Wea. Forecasting*, **18**, 585-599.

Huggel, A., W. Schmid, and A. Waldvogel, 1996: Raindrop size distributions and the radar bright band. *J. Appl. Meteor.,* **35**, 1688–1701.

Joss, J., and R. Lee, 1995: The application of radar-gauge comparisons to operational precipitation profile corrections. *J. Appl. Meteor*., **34**, 2612–2630.

Kitchen, M., R. Brown, and A. G. Davies, 1994: Real-time correction of weather radar data for the effects of bright band, range and orographic growth in widespread precipitation. *Quart. J. Roy. Meteor. Soc.,* **120,** 1231–1254.

Koistinen, J. 1991: Operational correction of radar rainfall errors due to the vertical reflectivity profile. *Preprints, 25th Int. Conf. On Radar Meteorology,* Paris, France, Amer. Meteor. Soc., 91–94.

Lakshmanan, V., A. Fritz, T. Smith, K. Hondl, and G. J. Stumpf, 2007: An automated technique to quality control radar reflectivity data. *J. Appl. Meteor*., **46**, 288–305.

Lhermitte, R. M., and D. Atlas, 1963: Doppler fall speed and particle growth in stratiform precipitation. *Preprints, 10th Radar Meteor. Conf.,* Washington DC, Amer. Meteor. Soc., 297–302.

Ryde, J. W., 1946: The attenuation and radar echoes produced at centimeter wavelengths by various meteorological phenomena. *Meteorological Factors in radio Wave Propagation,* Phys. Soc., 169–188.

Sánchez-Diezma, R., I. Zawadzki, R. and D. Sempere-Torres, 2000: Identification of the bright band through the analysis of volumetric radar data. *J. Geophy. Res,* **105**, 2225–2236.

Seo, D.-J., J. Breidenbach, R. Fulton, D. Miller, and T. O'Bannon, 2000: Real-time adjustment of range-dependent biases in WSR-88D rainfall estimates due to nonuniform vertical profile of reflectivity. *J. Hydrometeor.,* **1,** 222–240.

Smith, C. J., 1986: The reduction of errors caused by bright bands in quantitative rainfall measurements made using radar. *J. Atmos. Oceanic Tech.,* **3,** 129-141.

Smyth, T. J., and A. J. Illingworth, 1998: Radar estimates of rain-fall rates at the ground in bright band and non-bright band events. *Quart. J. Roy. Meteor. Soc.,* **124,** 2417-2434.

Stewart, R. E., J. D. Marwitz, J. C. Pace, and R. E. Carbone, 1984: Characteristics through the melting layer of stratiform clouds. *J. Atmos. Sci.,* **41,** 3227-3237.

Takeda, T., and Y. Fujiyoshi, 1978: Microphysical processes around melting layer in precipitating clouds as observed by vertically pointing radars. *J. Meteor. Soc. Japan,* **56,** 293-303.

Vignal, B., and W. F. Krajewski, 2001: Large-sample evaluation of two methods to correct range-dependent error for WSR-88D rainfall estimates. *J. Hydrometeor*., **2**, 490–504.

—, G. Galli, J. Joss, and U. Germann, 2000: Three methods to determine profiles of reflectivity from volumetric radar data to correct precipitation estimates. *J. Appl. Meteor*., **39**, 1715–1726.

—, H. Andrieu, and J. D. Creutin, 1999: Identification of vertical profiles of reflectivity from volume scan radar data. *J. Appl. Meteor*., **38**, 1214–1228.

Westrick, K. J., C. F. Mass, and B. A. Colle, 1999: The limitations of the WSR-88D radar network for quantitative precipitation measurement over coastal western United States. *Bull. Amer. Meteor. Soc.,* **80,** 2289-2298.

Wexler, R., and D. Atlas, 1956: Factors influencing radar echo intensities in the melting layer. *Quart. J. Roy. Meteor. Soc.,* **82,** 349-351.

Willis, P. T., and A. J. Heymsfield, 1989: Structure of the melting layer in mesoscale convective system stratiform precipitation. *J. Atmos. Sci.,* **46,** 2008-2025.